THE JOURNAL OF PHYSICAL CHEMISTRY C

ARTICLE

pubs.acs.org/JPCC

Photonic Crystal Geometry for Organic Polymer:Fullerene Standard and Inverted Solar Cells

Doo-Hyun Ko,[†] John R. Tumbleston,[‡] Walter Schenck,[†] Rene Lopez,[‡] and Edward T. Samulski*[,†]

[†]Department of Chemistry, University of North Carolina at Chapel Hill, Caudill and Kenan Laboratories CB 3290, Chapel Hill, North Carolina 27599-3290, United States

[‡]Department of Physics and Astronomy, University of North Carolina at Chapel Hill, Phillips Hall CB 3255, Chapel Hill, North Carolina 27599-3255, United States

Supporting Information

ABSTRACT: We describe a 2-D photonic crystal (PC) geometry that enhances the absorption of light for organic photovoltaic (OPV) cells relative to conventional planar cells. The PC geometry is developed by patterning an organic photoactive bulk heterojunction blend of P3HT (poly(3-hexylthiophene)) and PCBM (phenyl-C61-butyric acid methyl ester) via PRINT (pattern replication in nonwetting templates), a method that lends itself to large area fabrication of nanoscale features. Replication flexibility for various patterns and ranges of materials emphasizes the utility of PRINT for both inverted and standard OPV architectures. The optical properties of PC cells for different device architectures are investigated theoretically and experimentally in order to determine critical physical dimensions that influence device performance.

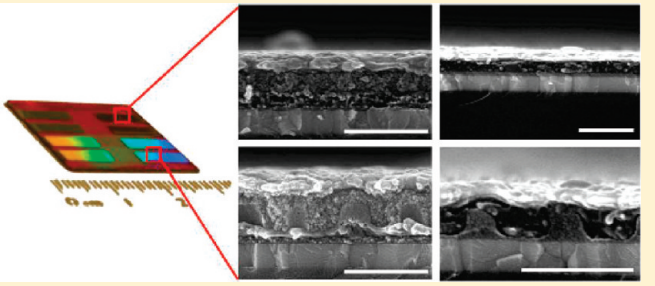

INTRODUCTION

Attempts to optimize both the optical and electrical requirements of the photoactive layer in organic photovoltaic (OPV) cells inevitably result in a compromise for photoactive layer thickness that limits efficiency.[1−3] A variety of light trapping schemes have been advanced to offset competing requirements: metal diffraction gratings,[4] collector mirrors,[5] buried nanoelectrodes,[6] microprism substrates,[7] and V-folded cell configurations.[8] In theory, embossing a photonic crystal (PC) nanopattern in the photoactive layer should improve absorption over a range of wavelengths because it may function as a resonant structure and low loss mirror.[9] However, complicated traditional processing has been the primary barrier to fabricating PC nanopatterns for enhancing the efficiencies of OPV cells. To date, only a limited number of 1-D periodic PC designs have been reported.[4,6,10−12] The intricacies of PC nanopatterns, the range of usable PV materials, and the device architecture can severely limit conventional lithographic routes to PC nanopatterns. We previously reported a method to fabricate a scalable, 2-D PC nanopattern in OPV devices with a facile processing strategy called PRINT.[13] However, in our initial work we were restricted to using a low-efficiency bulk heterojunction (BHJ) system, TDPTD (thermally deprotectable polythiophene derivatives):PCBM, due to the need to control the flash layer thickness (see Figure 2e). Thermal curing of TDPTD caused it to become insoluble and enabled us to separately form the flash layer by a spin-coating step prior to forming the PC layer. Herein, we show that the benefit of a PC geometry in OPV devices may be extended to standard BHJ materials (e.g., P3HT:PCBM)[14] in both standard and inverted[15] cell architectures where the PC geometry can be prepared by optimizing both the initial photoactive layer thickness to be patterned and the embossing pressure. A further extension to a PC tandem cell is also explored by inserting a robust photoactive layer (copper phthalocyanine) underneath the PC-patterned BHJ layer that optically compliments P3HT:PCBM. A device efficiency of 2.91% is realized, which is the highest performance reported for this new generation of OPV.

We illustrate the flexibility of our nanopattening methodology by demonstrating that PRINT is applicable to a variety of feature shapes and materials, and we explore nanopattern features that influence the absorption as a direct result of the PC phenomenon in both standard and inverted cell architectures. Then, we contrast OPV device performance of patterned PC cells with planar, unpatterned, control cells where we consider both the optical and the electrical characteristics of standard and inverted architectures. We show theoretically and experimentally that optical interference can markedly affect absorption in the photoactive layer and change absorption by as much as 90% depending on the thickness of layers adjacent to the photoactive BHJ. Excitation of resonant modes is observed in PC cells for both architectures. Also, we find that when absorption is maximized

Received: November 24, 2010
Revised: January 23, 2011
Published: February 21, 2011

for both PC and planar cells employing the P3HT:PCBM BHJ, a 13% enhancement is possible. This enhancement is achieved by optimizing the flash layer thickness in the PC nanopattern and the zinc oxide layer thickness. These parameters are investigated theoretically and experimentally in this paper. Further enhancement should be possible by tuning the parameters for optimal device performance, e.g., periodicity, height, and shapes of PC nanopatterns.[16,17]

EXPERIMENTAL SECTION

PT Device Fabrication. ITO (indium tin oxide)-coated glass was cleaned with acetone, isopropyl alcohol, and distilled water for 10 min each and then dried overnight in an oven (150 °C). The cleaned substrate was treated with UV ozone for 20 min (UVO Cleaner 42, Jelight Co. Inc.). The PEDOT:PSS (poly-(3,4-ethylenedioxythiophene):poly(styrenesulfonate), Baytron was filtered with a 0.45 μm PVDF filter, and then 35 nm of PEDOT:PSS was spin-coated onto the substrate and annealed for 10 min at 140 °C. The annealed sample was moved into an inert gas (purified nitrogen) glovebox. In order to prepare the PC layer, a solution containing P3HT (15 mg mL^{-1}) and PCBM (12 mg mL^{-1}) in chlorobenzene was spin-coated onto the PEDOT:PSS-coated substrate. The spin-casted layer was patterned by contacting a perfluoropolyether (PFPE) mold under pressure at 145 °C for 30 min, a variation of the PRINT methodology;[4,18] the planar cell was simultaneously fabricated by embossing the layer with a flat PFPE mold. The patterning step was followed by spin-coating various concentrations of nanocrystalline zinc oxide (*nc*-ZnO[19] in methanol to get the desired thickness of *nc*-ZnO film. Finally, the device was transferred into a vacuum chamber (2×10^{-6} Torr), and 100 nm Al was deposited on defined cell areas (12 mm^2). The device structures were characterized by SEM (Hitachi S-4700). The thickness of the planar photoactive layer in the control cells was held constant at 90 nm. The actual photoactive P3HT:PCBM layer in the PC cell consists of a flash layer (40 nm) covered by a hexagonal array of column-like features with a height of 180 nm, diameter of 220 nm, and a translational periodicity of 400 nm.

PT-Cu Device Fabrication. CuPC (copper phthalocyanine, 13 nm) was thermally deposited with 0.2 Å/s rate on ITO/PEDOT:PSS, and the PC and planar cells were fabricated on the same substrate by embossing the spin-coated P3HT:PCBM layer with a PFPE mold. Subsequently, *nc*-ZnO and Al were deposited in the same manner as for the PT device.

iPT Device Fabrication. The titanium oxide (TiO_2) sol−gel was prepared by the previously reported method.[20] The TiO_2 sol−gel was spin-casted on the cleaned ITO, and the film was annealed at 450 °C for 30 min to form crystalline TiO_2. The P3HT:PCBM solution was spin-coated on the TiO_2 layer (10 nm) and was embossed with PFPE at 145 °C for 30 min for planar and PC cells. Finally, the device was transferred into a vacuum chamber (2×10^{-6} Torr), and Ag/WO_3 layers were subsequently thermally deposited on both areas.

iPT-Ti Device Fabrication. The amorphous titanium oxide (TiO_x) nanopatterns were formed by embossing the prepared TiO_2 sol−gel[18] with PFPE mold and subsequently annealing the film at 150 °C for 90 min in air. The identical P3HT:PCBM solution was spin-coated on the patterned and planar TiO_x layer, and the devices were annealed at 145 °C for 30 min in a glovebox filled with inert gas. The device was completed by depositing Ag/WO_3 layers in a vacuum chamber (2×10^{-6} Torr).

RESULTS AND DISCUSSION

Replication of Nanopatterns. The PRINT method[13,18,21] (see Supporting Information Figure S1) was used to fabricate a precision PC nanopattern in P3HT:PCBM or in amorphous titanium oxide (TiO_x)[18] over large areas (2.50 cm × 1.25 cm). Earlier work from our laboratory illustrated the power of PRINT for nanopatterning a variety of materials.[18,21,22] Here we focus on patterns and materials that have utility in OPV cells. Figure 1 shows P3HT:PCBM and (TiO_x)[18] nanopatterns made using PRINT without any addition of surfactant that include triangular, square, rectangular, grating, and columnar feature shapes. For the standard OPV device, nanopatterned P3HT:PCBM was replicated on PEDOT:PSS coated ITO. In the case of inverted organic photovoltaic (iOPV) cells, TiO_x was patterned on an ITO substrate. All replicated patterns are periodic with PC-active dimensions on the order of the wavelength of visible light. Every nanopattern includes a "flash layer"—a thin layer below and surrounding each feature that interconnects the array of features (see Figure 2e). The hexagonal array of column-like features was chosen for our OPV study as its 2-D periodicity is capable of enhancing absorption of both polarizations of light. Moreover, a 400 nm periodicity when coupled with the inherent optical properties of the nanopatterned materials resulted in resonant modes near the band edge of P3HT:PCBM. We will discuss the resonant modes below in detail.

OPV and iOPV Device Fabrication. Nanopatterned P3HT:PCBM or TiO_x was incorporated into OPV and iOPV devices in a manner that yields a refractive index contrast between the two adjacent nanopatterned layers. This was achieved by "backfilling" a low index material into the nanopatterned BHJ layer in an OPV or incorporating the BHJ layer into the nanopatterned metal oxide of an iOPV. For instance, if a 2-D PC topography is embossed in the BHJ layer (P3HT:PCBM), a relatively high refractive index mixture (~2.1 at 550 nm), it must be surrounded by a relatively low refractive index material such as nanocrystalline zinc oxide (*nc*-ZnO; ~1.46 over the wavelength range 400−800 nm) in order to exhibit PC behavior (see Supporting Information Figure S2). Likewise, the patterning of low index TiO_x when surrounded by P3HT:PCBM has the requisite PC refractive index contrast (see Supporting Information Figure S2). For some OPV devices where only partial filling of *nc*-ZnO occurred and for iOPV devices with thin overlayers of WO_3, a conformal evaporated metal electrode partially filled the nanopatterned topography and resulted in photonic effects.

The successive layer configurations of devices employed in this study are shown in Table 1. The embossed layer in each cell is indicated by "planar" or "PC" for flat and nanopatterned cells, respectively. The PC nanopatterned material is boldfaced in the standard and inverted devices, and each device has eight simultaneously fabricated cells with 12 mm^2 active area (see Figure 2a). The photoactive material (P3HT:PCBM) was nanopatterned on PT, PT-Cu, and iPT devices, whereas the TiO_x was nanopatterned on the iPT-Ti device.

The thickness of the overlayer (d_i) used for refractive index contrast varies with position: d_1 is thickness in the planar cell, the thickness of backfill between PC features is denoted by d_2, and d_3 is the overlayer above the PC columnar features (see Figure 2d). The d_i values are important variables that influence the absorption performance, and the effect of these values will be discussed below. All devices were prepared on an ITO (150 nm) substrate

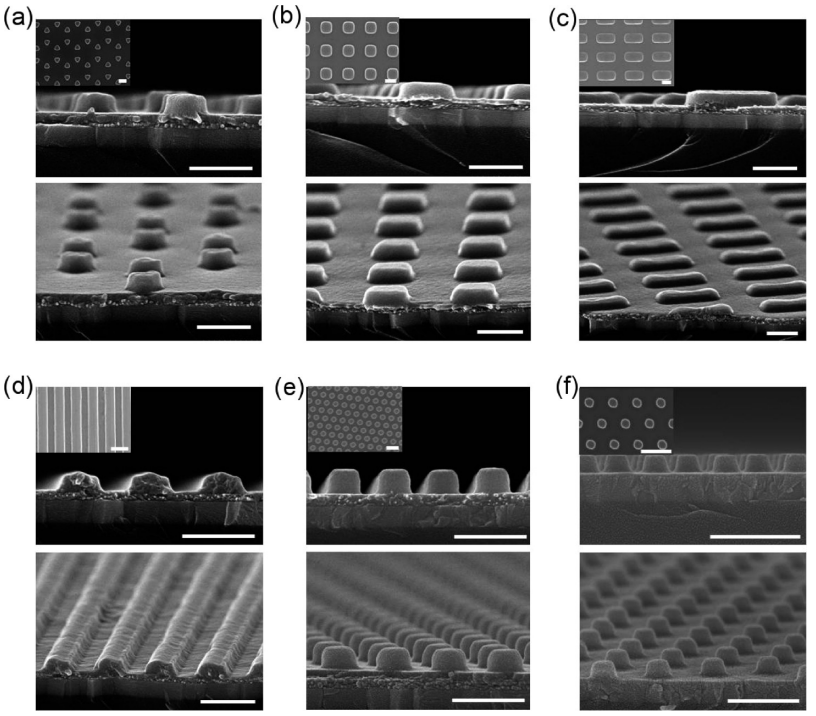

Figure 1. SEM (scanning electron microscope) pictures for P3HT:PCBM replicas of PC nanopatterns using PRINT to fabricate features having a range of geometries: (a) hexagonal, (b) square, (c) rectangular, (d) linear grating, and (e) rows of columns. All patterns (a−e) are embossed into PEDOT:PSS on an ITO substrate (on glass). In (f), columnar hexagonal TiO_x nanopatterns were prepared on an ITO substrate. SEM pictures show respectively cross-section views (top) and oblique views (bottom) with corresponding normal views (insets). All scale bars are 500 nm.

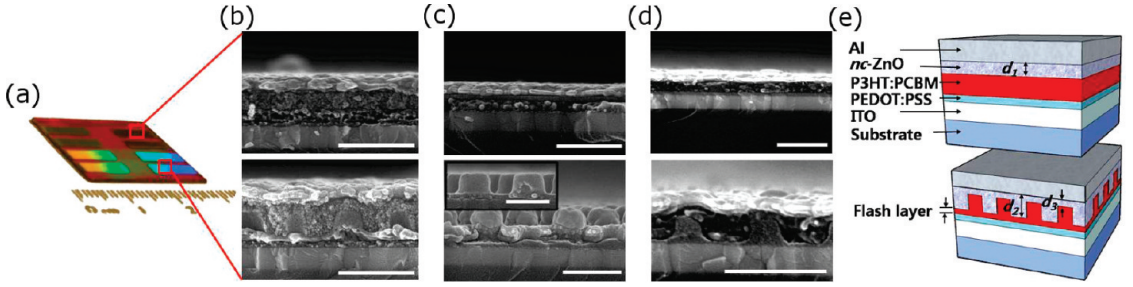

Figure 2. OPV cell cross sections. (a) Photograph of planar (rear of device) and iridescent PC cells on the same device. (b, c, d) SEM pictures showing the cross sections of planar (top) and PC cells (bottom). (e) Schematic of planar and PC device architectures. The respective device layer sequences are (b) PT (ITO/PEDOT:PSS/P3HT:PCBM/*nc*-ZnO/Al), (c) iPT (ITO/TiO_2/P3HT:PCBM/WO_3/Ag), and (d) iPT-Ti (ITO/TiO_x/P3HT:PCBM/WO_3/Ag). The PC geometries were prepared by patterning either the P3HT:PCBM (b, c) or the TiO_x layer (d). The inset outlined in black (c) shows a cross section of the nanopatterned P3HT:PCBM before WO_3/Ag deposition. All scale bars are 500 nm.

where PEDOT:PSS (35 nm) and Al (100 nm) were used for the standard devices.

Figure 2a shows a photograph of planar and iridescent PC cells on a device. SEM cross sections (Figure 2b−d) of planar and nanopatterned PC cells and schematics of both cell types (Figure 2e) are shown for the for PT device. Each designated device (PT, PT-Cu, iPT, and iPT-Ti) has a single architecture (standard or inverted succession of layers) and both PC and planar cells, four of each type (see Figure 2a). Placing both flat and nanopatterned cell types on the same device substrate ensured that both types were subjected to identical fabrication steps and thermal histories. Also, the simultaneous fabrication ensures that both cell types have equivalent volumes of each respective layer component. Moreover, to avoid potential surface contamination errors when contrasting the performance of the two cell types during the PRINT step, the planar cell was also "embossed" with a featureless flat perfluoroelastomer (PFPE) film while the PC cell was embossed with the nanopatterned PFPE mold. In the PC cell, the flash layer (see Figure 2e) was intrinsically introduced during the PRINT process. The thickness of the flash layer affects the absorption of incident light, so in this study, the flash layer thickness was fixed at 40 nm. (The optical effect of the flash layer will be discussed below.) Further details about the fabrication processes for each device are described in the Experimental section.

Optical Performance of PC and Planar Cells. In order to characterize the optical performance of PC and planar cells, the reflection spectrum of each cell was measured on the same substrate using s-polarized light under 15° incidence. While

dx.doi.org/10.1021/jp1112087 |*J. Phys. Chem. C* 2011, 115, 4247–4254

Table 1. Configurations of PC and Planar Cells[a]

OPV device type	name	architecture	dimension (nm) planar,[b] PC[c]	dimension (nm) d_1, d_2, d_3
standard	PT	ITO/PEDOT:PSS/**P3HT:PCBM**/*nc*-ZnO/Al	90, 180	110, 195, 20
standard	PT-Cu[d]	ITO/PEDOT:PSS/CuPC/**P3HT:PCBM**/*nc*-ZnO/Al	80, 170	90, 200, 20
inverted	iPT[e]	ITO/TiO_2/**P3HT:PCBM**/WO_3/Ag	95, 180	10, 10, 10
inverted	iPT-Ti[f]	ITO/**TiO_x**/P3HT:PCBM/WO_3/Ag	40, 135	95, 150, 40

[a] For PC cells, the hexagonal array of column-like features where the radius is 110 nm and the periodicity is 400 nm are prepared. [b] Thickness of the embossed layer for planar cell. [c] Height of the replicated nanopatterns for PC cell. [d] For PT-Cu devices, 13 nm of CuPC (copper phthalocyanine) was incorporated. [e] For iPT devices, TiO_2 (10 nm) and Ag (120 nm) were incorporated. [f] For iPT-Ti devices, WO_3 (30 nm) and Ag (100 nm) were deposited.

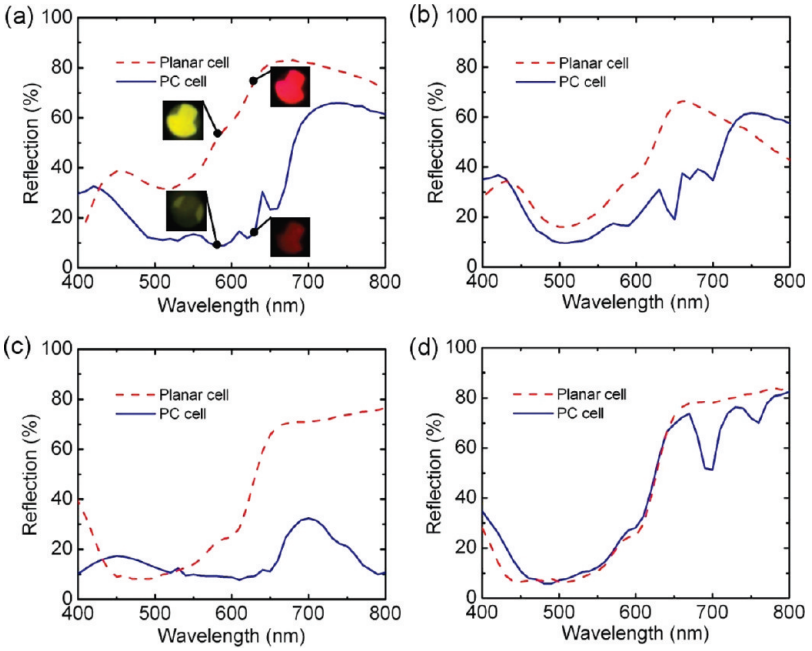

Figure 3. Zeroth-order reflection for PC and planar cells for s-polarized light at 15° incidence for standard cell architectures ((a) PT and (b) PT-Cu) and inverted cell architectures ((c) iPT and (d) iPT-Ti). See Table 1 for each device's architecture. The insets of (a) show camera image differences between PC and planar cells, a coarse indicator of the absorption enhancement for PC cells in the device.

absorption in the photoactive blend cannot be measured directly, the reflection spectra are an effective indicator of total absorption losses including those losses due to resonant modes. This is because there is negligible transmission through the metal electrode and minimal coherent scattering close to normal incidence where the diffractive/iridescence effects are only appreciable at large angles. The reflection measurement is also used to determine an appropriate optical model for the PC and planar cells where the distribution of absorption losses in each cell material can be quantified. Figure 3 shows reflection spectra for PC and planar cells for different device architectures and material components. For the PT and PT-Cu devices (Figure 3a, b) the PC cells show lower reflection and correspondingly higher absorption relative to planar cells on the same substrate. The loss of reflection at certain wavelengths is even apparent to the naked eye (insets of Figure 3a). On the other hand, the iOPV devices have similar reflection spectra for both planar and PC cells, especially in the visible region as shown in Figure 3c,d. The differences noted between PC and planar cells for different device types arise from variability in optical interference. In other words, the total absorption in the cells is controlled by all physical

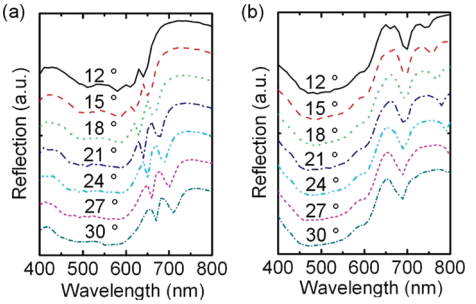

Figure 4. Angular-dependent reflection spectra for the PC cell in (a) PT and (b) iPT-Ti devices. The dips in reflection between 600 and 800 nm as the incident angle changes indicate the excitation of resonant modes.

dimensions such as layer (PV material, low index material, ITO, etc.) thicknesses along with the optical properties of all device materials. Especially for PC cells, physical dimensions such as height and periodicity of the nanopatterned layer plays an important role.[23−25] The relationship between reflection and

dx.doi.org/10.1021/jp1112087 |J. Phys. Chem. C 2011, 115, 4247–4254

optical absorption of each cell in the photoactive material, P3HT:PCBM, will be discussed below in further detail.

Excitation of Resonant Modes. The unique sharp features in the reflection spectra exhibited by PC cells in Figure 3 are characteristic of resonant modes, which trap incident light in the cell. The presence of these modes is confirmed in Figure 4 by the blue- and red-shifts as the incident angle changes from 12° to 30°. Even though the reduction in reflection is significant from the resonant modes, P3HT:PCBM becomes essentially transparent around 650 nm. Thus, any additional absorption due to resonant mode excitation can only occur if they exist for wavelengths lower than the band edge. In this case, the contribution to the overall photocurrent is small due to the limited coupling of the resonant modes to the photoactive layer. This is clear for the PT device because the modes are still visible in the reflection spectra even as they red-shift past the band edge of P3HT:PCBM. Even so, by controlling PC dimensions the excitation of resonant modes in PC cells offers the possibility to increase photocurrent by appropriately matching the modes to the absorption spectrum of the active PV materials.[23,24] For instance, the photon flux of the solar spectrum is highest in the near-IR and could be effectively captured with low-band-gap materials[26] having a tuned PC cell geometry.

Characterization of Device Performance. Even though cell reflection characteristics are a good indicator of total cell absorption and resonant mode excitation, an optical model of the cell is an invaluable tool to quantify absorption in various layers, e.g., the photoactive layer and other lossy components like PEDOT:PSS, ITO, and Al. Furthermore, resonant modes may be partially or fully trapped in "inert" layers like PEDOT:PSS and ITO, thereby creating no additional photocurrent.[13] By fitting a solution to Maxwell's equations to the measured reflection data,[13] the optical redistribution of incident light in the PT device is calculated for PC and planar cells under normal incidence (Figure 5a,b; see Table 1 for device architecture). Input into the model includes the optical properties of all materials as measured via spectroscopic ellipsometry (see Supporting Information Figure S2). Herein, we assume all materials to be isotropic even though anisotropy has been noted in device materials[27,28] like PEDOT:PSS. The isotropic model serves as a good approximation to the devices studied here, especially since the optical electric fields for our measurements (s-polarization at 15°) and simulations (normal incidence) are only dictated by the measured in-plane optical properties. For the PC cell, absorption in P3HT:PCBM is approximately equal between the thin 40 nm flash layer (42%) and 180 nm tall columns (58%), while Al and ITO also contribute to absorption above 650 nm where P3HT:PCBM is essentially transparent.

Absorption in the photoactive layer is the only optical loss that leads to the creation of excitons; this is quantified by calculating the total exciton generation rate. The latter is obtained by multiplying the fraction of absorption in P3HT:PCBM from the optical redistribution (see Figure 5a,b) by the AM 1.5 solar spectrum and integrating over the wavelengths where P3HT:PCBM is absorptive. This is then multiplied by the thickness of the photoactive layer or, in the case of PC cells, a P3HT:PCBM film thickness with an equivalent volume of the flash and nanopatterned layers. This calculation indicates that P3HT:PCBM absorption in the PC cell is about 50% higher relative to the planar cell (PC cell: 6.38×10^{20} s^{-1} m^{2}; planar cell: 4.15×10^{20} s^{-1} m^{2}). A similar difference is noted in the $J-V$ measurement. Under 85 mW/cm^2 illumination, the J_{sc} for PC cells (8.93 mA/cm^2) is 40% higher than the planar cell (6.36 mA/cm^2), as shown in Figure 5c. It should be noted that the observed efficiency for the PC cell is 2.91% with open-circuit voltage (V_{oc}) of 0.61 V and a 46% fill factor (FF).

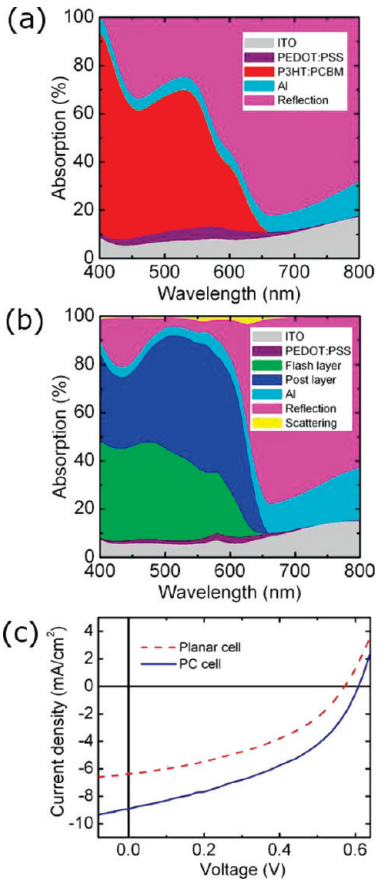

Figure 5. Optical redistributions at normal incidence for (a) planar and (b) PC cells for PT device under normal incidence (see Table 1 for device architecture). The *nc*-ZnO layer is transparent for wavelengths above 400 nm, so its absorptions profile is not shown as it is equal to zero. (c) Current density vs voltage ($J-V$) behavior for PC and planar cells where the PC cell shows higher absorption compared to the planar cell, which follows the prediction by the optical model.

Device Performance Parameters: *nc*-ZnO Thickness. Even though the PC cells in the PT device shows a greater absorption and J_{sc} relative to the planar cell fabricated on the same substrate, optical interference plays a major role in determining the absorption and the resulting J_{sc} for both PC and planar cells. For instance, the thickness of the transparent, PC backfill material, *nc*-ZnO, affects absorption, making it important to explore a range of backfill thicknesses to ascertain the maximum absorption.[16,29] Figure 6a shows the total exciton generation rate calculated with the optical model as a function of *nc*-ZnO flash thickness (d_3) and film thickness (d_1) for PC and planar cells, respectively (see Figure 2e). For the PC cell, the *nc*-ZnO thickness between the columns (d_2) is fixed to the column height (180 nm). The experimental data points (symbols in Figure 6a) mark fabricated devices where simulated reflection spectra have been fitted to the measured reflection by varying physical dimensions. Using the best fit optical model, the total exciton generation rate can be determined. The calculations (curved lines) in Figure 6a are performed using ITO = 150 nm and PEDOT = 42 nm, which are derived from the average layer thickness (ITO, PEDOT:PSS, etc.) for all devices where slight

dx.doi.org/10.1021/jp1112087 |J. Phys. Chem. C 2011, 115, 4247–4254

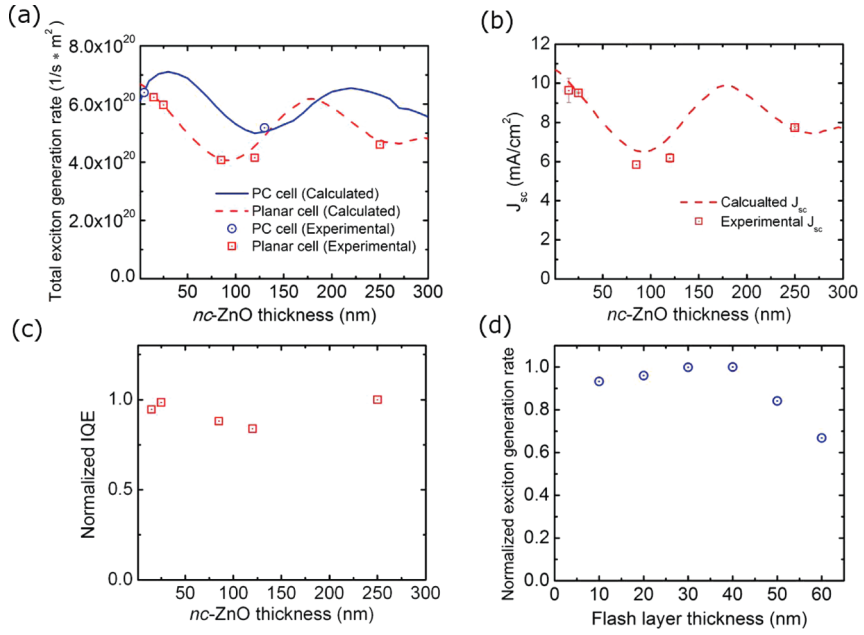

Figure 6. (a) Total exciton generation rate as a function of *nc*-ZnO overlayer thickness (d_3) and planar film thickness (d_1) for PC and planar cells, respectively. Symbols correspond to fabricated devices that lie along the calculated curve for all *nc*-ZnO thicknesses between 0 and 300 nm. (b) Calculated short circuit current (J_{sc}) as a function of *nc*-ZnO film thickness for planar cells using the total exciton generation rates in (a). Measured values are given as symbols. (c) The normalized internal quantum efficiency is relatively independent of *nc*-ZnO thickness. (d) The normalized exciton generation rate for fixed *nc*-ZnO thickness (d_3 = 20 nm) is a strong function of the flash layer thickness.

variations were noted (see Table 1 for other dimensions). Absorption for both PC and planar cells oscillates with *nc*-ZnO thickness where a ~90% variation from maximum to minimum is noted for planar cells. This is a critical point and supports our methodology of making devices with a range of *nc*-ZnO thicknesses because simply making one device could lead to simultaneous fabrication of maximum absorbing PC cells and minimum absorbing planar cells (or vise versa) on the same device substrate. This is approximately the case for the device presented in Figure 5. However, comparing the peak values of the exciton generation rate for each cell type suggests there is a 13% absorption enhancement for PC cells. Also, further enhancement would be possible with an idealized geometry for PC nanopatterns in P3HT:PCBM devices.[17]

Using the calculated absorption values (total exciton generation rate), the J_{sc} in the photoactive layer is calculated assuming an internal quantum efficiency (IQE) of unity (see Figure 6b).[30] The variation in the absorption with *nc*-ZnO thickness impacts the calculated J_{sc} and is compared with experimental J_{sc} (symbols in Figure 6b) for various *nc*-ZnO thickness cells. As shown in Figure 6b, the experimental values are parallel to the calculated variation. Since the *nc*-ZnO is an additional electron transporting layer, its thickness may affect the electrical device performance. The IQE is a measure of the electrical processes in the cells at short circuit and is calculated by dividing the total exciton generation rate by the measured J_{sc}. Importantly, the IQE is relatively constant regardless of *nc*-ZnO thickness as shown in Figure 6c. Therefore, it is determined that the thickness of the high conductivity *nc*-ZnO is not a critical parameter for device performance, which in turn indicates that the observed change in J_{sc} with *nc*-ZnO thickness is an optical effect.

Device Performance Parameters: Flash Layer Thickness. Another factor that affects absorption in the PC cell is the flash layer thickness. The PV-active blend layer thickness is 90 nm in planar cells. A comparable blend volume in the PC cell must be partitioned between the flash layer and the PC nanopattern. In Figure 6d, normalized exciton generation rates for PC cells are obtained as a function of flash layer thickness at a fixed *nc*-ZnO thickness (d_3 = 20 nm). A thinner flash layer will allow more blend to be used in the patterned PC layer, which, in turn, increases the photonic activity as shown in Figure 6d. PC cells with high aspect ratio patterns are less sensitive to *nc*-ZnO thickness (less variation in absorption with thickness) (see Supporting Information Figure S3). However, thin flash layers are susceptible to shorting via direct contact between the *nc*-ZnO and PEDOT:PSS interface. Therefore, control of the flash layer thickness is crucial for both electrical and optical performance. Herein, the thickness of the flash layer was controlled by the applied pressure during the PFPE embossing process in conjunction with the initial thickness of the photoactive blend to be patterned. We observed that a torque of 1.69 N m with our embossing setup consistently yielded a 40 nm flash layer in the PC cells. Earlier we reported that the flash layer thickness could be controlled by preparing an insoluble PV film layer by thermal curing.[13] Alternately, the incorporation of an additional layer underneath the photoactive layer is an option if it is conductive and does not hinder carrier transport. Also, such a layer's absorption spectrum should not significantly overlap that of the photoactive layer.

In this spirit, the PT-Cu device was fabricated with various *nc*-ZnO thickness by incorporating a thin CuPC layer (13 nm) underneath the photoactive P3HT:PCBM layer in both PC and planar cells. The CuPC has relatively high glass temperature[31] and should not be modified during the PRINT process at 145 °C. Furthermore, the IR region of the solar spectrum where P3HT:PCBM cannot contribute to photocurrent generation is absorbed by CuPC, which in turn has low absorption bands between 400 and 550 nm where P3HT:PCBM absorbs strongly

(see Supporting Information Figure S4). Also, the CuPC HOMO (3.5 eV) and LUMO (5.2 eV)[32] are well matched to the P3HT:PCBM energy levels for favorable carrier transport. The CuPC layer protects against direct shorting between PEDOT:PSS and *nc*-ZnO in the PC cell including those PC cells with a thin flash layer of P3HT:PCBM.

As shown in Figure 3b, the reflection spectra for PC and planar cells in the fabricated PT-Cu device indicate an enhanced absorption for the PC cells. Also, this result is confirmed by the J_{sc} measurement where the J_{sc} for a PC cell is 5.9 ± 0.11 mA/cm^2 (whereas the planar cell on the same device exhibited a smaller J_{sc} (4.8 ± 0.13 mA/cm^2). Although the absolute values of the observed J_{sc} are lower than in optimized P3HT:PCBM devices[1,29] without a CuPC layer, the result supports the electrical isolation capability of CuPC is advantageous for device performance. However, it is worth mentioning the reason for the low performance for these cells. This could be due to both optical and electrical causes associated with using a relatively thick CuPC layer: First, the small overlap of the absorption spectra of a thick CuPC layer with that of P3HT:PCBM over a wavelength range of 550−650 nm (see Supporting Information Figure S4) would reduce the incident photons on the latter. Second, a short-lived exciton created in the thick CuPC layer may not diffuse to the CuPC/P3HT:PCBM interface. Thus, the 13 nm thick CuPC layer may hamper device performance. The influence of the CuPC thickness in OPV devices on device performance was recently reported to be a critical parameter for optimization.[33] Also, the use of a relatively thin photoactive layer of P3HT:PCBM (80 nm) in our devices might reduce photocurrents. Thus, the PC effect for the CuPT devices should be further investigated with optimized layer thicknesses for *nc*-ZnO, CuPC, and the photoactive layer (P3HT:PCBM). Also, the absorption in the IR region by the CuPC layer may enable one to apply this design to a tandem cell architecture.[32,33]

CONCLUSIONS

We reiterate that PRINT is a powerful way to simply fabricate accurate photonic crystals over a large area in a controlled way. Nanopatterns with different shapes, dimensions, periodicities, and material composition in PC geometries are readily embossed in OPV devices. In conjunction with appropriately contrasting refractive indices at the interface of the nanopatterns, the geometries exhibit photonic effects for both standard OPV and iOPV. The optical interference in PC cells is strongly affected by not only physical dimensions, such as height and periodicity of the nanopatterned layer, but also by the device architecture, standard versus inverted. We show how an enhanced absorption derived from a photonic effect directly leads to an enhancement of device performance. We envision further improvements in PC solar cells when the nanopattern is optimized in PV-active materials that absorb more efficiently in the near-infrared where resonant modes are commonly excited.

ASSOCIATED CONTENT

Supporting Information. Description of fabrication details, optical properties of the used films, and calculated absorption performance according to the flash layer thickness. This material is available free of charge via the Internet at http://pubs.acs.org.

AUTHOR INFORMATION

Corresponding Author
*E-mail: et@unc.edu.

ACKNOWLEDGMENT

Support for this work is from NSF (Solar: DMR-0934433) and UNC-Chapel Hill Institute for the Environment (Carolina Energy Fellows Program). Acknowledgment is also made to the donors of The American Chemical Society Petroleum Research Fund (No.49187-DNI10) for partial support of this research. We thank Robert Brady, Wei You, Stuart Williams, and Meredith Hampton for stimulating conversations.

REFERENCES

(1) Li, G.; Shrotriya, V.; Huang, J.; Yao, Y.; Moriarty, T.; Emery, K.; Yang, Y. *Nature Mater.* **2005**, *4*, 864.
(2) Li, G.; Shrotriya, V.; Yao, Y.; Yang, Y. *J. Appl. Phys.* **2005**, *98*, 043704.
(3) Coakley, K. M.; McGehee, M. D. *Chem. Mater.* **2004**, *16*, 4533.
(4) Roman, L. S.; Inganäs, O.; Granlund, T.; Nyberg, T.; Svensson, M.; Andersson, M. R.; Hummelen, J. C. *Adv. Mater.* **2000**, *12*, 189.
(5) Peumans, P.; Bulovic, V.; Forrest, S. R. *Appl. Phys. Lett.* **2000**, *76*, 2650.
(6) Niggemann, M.; Glatthaar, M.; Gombert, A.; Hinsch, A.; Wittwer, V. *Thin Solid Films* **2004**, *451*−*452*, 619.
(7) Niggemann, M.; Glatthaar, M.; Lewer, P.; Müller, C.; Wagner, J.; Gombert, A. *Thin Solid Films* **2006**, *511*−*512*, 628.
(8) Rim, S.-B.; Zhao, S.; Scully, S. R.; McGehee, M. D.; Peumans, P. *Appl. Phys. Lett.* **2007**, *91*, 243501.
(9) Duche, D.; Escoubas, L.; Simon, J.-J.; Torchio, P.; Vervisch, W.; Flory, F. *Appl. Phys. Lett.* **2008**, *92*, 193310.
(10) Cocoyer, C.; Rocha, L.; Sicot, L.; Geffroy, B.; de Bettignies, R.; Sentein, C.; Fiorini-Debuisschert, C.; Raimond, P. *Appl. Phys. Lett.* **2006**, *88*, 133108.
(11) Na, S.-I.; Kim, S.-S.; Kwon, S.-S.; Jo, J.; Kim, J.; Lee, T.; Kim, D.-Y. *Appl. Phys. Lett.* **2007**, *91*, 173509.
(12) Kim, M.-S.; Kim, J.-S.; Cho, J. C.; Shtein, M.; Guo, L. J.; Kim, J. *Appl. Phys. Lett.* **2007**, *90*, 123113.
(13) Ko, D.-H.; Tumbleston, J. R.; Zhang, L.; Williams, S.; DeSimone, J. M.; Lopez, R.; Samulski, E. T. *Nano Lett.* **2009**, *9*, 2742.
(14) Ma, W.; Yang, C.; Heeger, A. J. *Adv. Mater.* **2007**, *19*, 1387.
(15) Chen, L.-M.; Hong, Z.; Li, G.; Yang, Y. *Adv. Mater.* **2009**, *21*, 1434.
(16) Tumbleston, J. R.; Ko, D.-H.; Samulski, E. T.; Lopez, R. *Opt. Express* **2009**, *17*, 7670.
(17) Tumbleston, J. R.; Ko, D.-H.; Samulski, E. T.; Lopez, R. *Appl. Phys. Lett.* **2009**, *94*, 043305.
(18) Hampton, M. J.; Williams, S. S.; Zhou, Z.; Nunes, J.; Ko, D.-H.; Templeton, J. L.; Samulski, E. T.; DeSimone, J. M. *Adv. Mater.* **2008**, *20*, 2667.
(19) Beek, W. J. E.; Wienk, M. M.; Kemerink, M.; Yang, X.; Janssen, R. A. J. *J. Phys. Chem. B* **2005**, *109*, 9505.
(20) Kim, J. Y.; Kim, S. H.; Lee, H. H.; Lee, K.; Ma, W.; Gong, X.; Heeger, A. J. *Adv. Mater.* **2006**, *18*, 572.
(21) Rolland, J. P.; Maynor, B. W.; Euliss, L. E.; Exner, A. E.; Denison, G. M.; DeSimone, J. M. *J. Am. Chem. Soc.* **2005**, *127*, 10096.
(22) Gratton, S. E. A.; Williams, S. S.; Napier, M. E.; Pohlhaus, P. D.; Zhou, Z.; Wiles, K. B.; Maynor, B. W.; Shen, C.; Olafsen, T.; Samulski, E. T.; DeSimone, J. M. *Acc. Chem. Res.* **2008**, *41*, 1685.
(23) Gippius, N. A.; Tikhodeev, S. G.; Ishihara, T. *Phys. Rev. B* **2005**, *72*, 045138.
(24) Andreani, L. C.; Gerace, D. *Phys. Rev. B* **2006**, *73*, 235114.
(25) Ferry, V. E.; Verschuuren, M. A.; Li, H. B. T.; Schropp, R. E. I.; Atwater, H. A.; Polman, A. *Appl. Phys. Lett.* **2009**, *95*, 183503.

(26) Peet, J.; Kim, J. Y.; Coates, N. E.; Ma, W. L.; Moses, D.; Heeger, A. J.; Bazan, G. C. *Nature Mater.* **2007**, *6*, 497.
(27) Pettersson, L. A. A.; Ghosh, S.; Inganäs, O. *Org. Electron.* **2002**, *3*, 143.
(28) Chuang, S.-Y.; Chen, H.-L.; Lee, W.-H.; Huang, Y.-C.; Su, W.-F.; Jen, W.-M.; Chen, C.-W. *J. Mater. Chem.* **2009**, *19*, 5554.
(29) Ma, W.; Yang, C.; Gong, X.; Lee, K.; Heeger, A. J. *Adv. Funct. Mater.* **2005**, *15*, 1617.
(30) Gilot, J.; Barbu, I.; Wienk, M. M.; Janssen, R. A. J. *Appl. Phys. Lett.* **2007**, *91*, 113520.
(31) Lee, Y.-J.; Lee, H.; Byun, Y.; Song, S.; Kim, J.-E.; Eom, D.; Cha, W.; Park, S.-S.; Kim, J.; Kim, H. *Thin Solid Films* **2007**, *515*, 5674.
(32) Zhang, C.; Tong, S. W.; Jiang, C.; Kang, E. T.; Chan, D. S. H.; Zhu, C. *Appl. Phys. Lett.* **2008**, *92*, 083310.
(33) Zhang, C.; Tong, S. W.; Jiang, C.; Kang, E. T.; Chan, D. S. H.; Zhu, C. *Appl. Phys. Lett.* **2008**, *93*, 043307.